


A kinase-dependent role for Haspin in antagonizing Wapl and protecting mitotic centromere cohesion

Cai Liang[†], Qinfu Chen[†], Qi Yi, Miao Zhang, Haiyan Yan, Bo Zhang, Linli Zhou, Zhenlei Zhang, Feifei Qi, Sheng Ye & Fangwei Wang^{*} 

Abstract

Sister-chromatid cohesion mediated by the cohesin complex is fundamental for precise chromosome segregation in mitosis. Through binding the cohesin subunit Pds5, Wapl releases the bulk of cohesin from chromosome arms in prophase, whereas centromeric cohesin is protected from Wapl until anaphase onset. Strong centromere cohesion requires centromeric localization of the mitotic histone kinase Haspin, which is dependent on the interaction of its non-catalytic N-terminus with Pds5B. It remains unclear how Haspin fully blocks the Wapl–Pds5B interaction at centromeres. Here, we show that the C-terminal kinase domain of Haspin (Haspin-KD) binds and phosphorylates the YSR motif of Wapl (Wapl-YSR), thereby directly inhibiting the YSR motif-dependent interaction of Wapl with Pds5B. Cells expressing a Wapl-binding-deficient mutant of Haspin or treated with Haspin inhibitors show centromeric cohesion defects. Phospho-mimetic mutation in Wapl-YSR prevents Wapl from binding Pds5B and releasing cohesin. Forced targeting Haspin-KD to centromeres partly bypasses the need for Haspin–Pds5B interaction in cohesion protection. Taken together, these results indicate a kinase-dependent role for Haspin in antagonizing Wapl and protecting centromeric cohesion in mitosis.

Keywords cohesin; Haspin; Pds5B; sister-chromatid cohesion; Wapl

Subject Categories Cell Cycle; Post-translational Modifications, Proteolysis & Proteomics; Signal Transduction

DOI 10.15252/embr.201744737 | Received 2 July 2017 | Revised 17 October 2017 | Accepted 19 October 2017 | Published online 14 November 2017

EMBO Reports (2018) 19: 43–56

Introduction

Sister-chromatid cohesion is mediated by the multi-subunit cohesin complex, which can entrap DNA inside its ring [1]. Precise regulation of sister-chromatid cohesion is fundamental for the fidelity of chromosome segregation [2]. In vertebrates, cohesin is removed from chromosomes in two steps during mitosis [3,4]. Through binding multiple cohesin subunits [5–9], Wapl releases the bulk of

cohesin from chromosome arms during prophase to allow sister-chromatid resolution [7,8]. Previous studies suggest that Wapl uses its YSR motif (with the consensus of K/R-S/T-YSR) or FGF motifs to associate with Pds5 and open a DNA exit gate in the cohesin ring [6,10–18]. Centromeric cohesin is protected from this removal activity until its proteolytic cleavage by the protease Separase at anaphase onset [3,19–21].

During chromosome bi-orientation, strong centromeric cohesion is critical to resist the spindle pulling force at sister kinetochores. Weak cohesion at centromeres causes premature chromatid separation (PCS) and chromosome missegregation, leading to chromosomal instability [22,23]. In contrast to the well-studied function of Sgo1 in the maintenance of sister-chromatid cohesion in mitosis [24–35], the role of the mitotic histone kinase Haspin in protecting centromeric cohesion [36] has only been recently ascertained [37,38].

Haspin consists of an unstructured non-catalytic N-terminal region and an atypical kinase domain in the C-terminus. Histone H3 is the only currently known endogenous substrate of Haspin [39]. Phosphorylation of H3-T3 (H3pT3) during mitosis by Haspin promotes inner centromeric localization of the chromosomal passenger complex (CPC) [40–42], which facilitates chromosome bi-orientation [43–45]. Haspin uses a N-terminal YSR-like Pds5-interacting motif (PIM) to bind Pds5 [37,38], which is required for centromeric enrichment of Haspin and H3pT3 [37,38,41,46]. Mutations in the PIM of Haspin disrupting its interaction with Pds5 cause weakened centromeric cohesion [37,38], indicating a requirement for the Haspin–Pds5B interaction in cohesion protection. The YSR (or YSR-like)-containing PIMs in Wapl and Haspin compete for Pds5B binding at least *in vitro* [37], suggesting one plausible mechanism for Haspin in antagonizing Wapl. However, it remains to be elucidated how Haspin fully blocks the Wapl–Pds5B interaction to ensure strong cohesion at mitotic centromeres. For example, it is unknown whether, and how, the Haspin kinase domain (Haspin-KD) may contribute to centromeric cohesion protection in mitosis.

Here, we describe and functionally characterize a novel interaction between Haspin and Wapl. We show that Haspin-KD binds and phosphorylates the YSR motif of Wapl (Wapl-YSR), thereby directly blocking the YSR motif-dependent Wapl–Pds5B interaction

at centromeres. This study reveals Haspin as a key factor that provides a unique means of protecting centromeric cohesion in mitosis.

Results and Discussion

Haspin-KD contributes to Wapl inhibition and centromeric cohesion protection in mitosis

Sgo1 protects centromeric cohesion mainly by antagonizing the cohesin release activity of Wapl, either directly or indirectly [7,8,26–28,30,31,47]. Haspin overexpression largely bypasses the requirement for Sgo1 in maintaining sister-chromatid cohesion during mitosis [36,37], indicating that both Haspin and Sgo1 are Wapl antagonists. However, when exogenously overexpressed as a SFB-fusion protein (SFB is a triple tag of S-tag, Flag-tag, and streptavidin-binding peptide) (Figs 1A and EV1A), the N-terminal region (amino acid residues 1–469) of Haspin (SFB-Haspin-N469) was defective in suppressing mitotic arrest (Fig 1B) and PCS (Figs 1C and EV1B) induced by Sgo1 depletion, while similar levels of wild-type (WT) SFB-Haspin were largely able to suppress these mitotic defects. Thus, overexpression of the N-terminal region of Haspin alone, while capable of binding Pds5B [37], cannot prevent the strong cohesion loss caused by Sgo1 depletion, suggesting a contribution of Haspin-KD to Wapl inhibition in mitosis.

Cells with chromosomal instability and weak cohesion undergo PCS to various extents, particularly during prolonged metaphase with sustained bipolar kinetochore tension [48,49]. As we recently reported, HeLa-derived Haspin-knockout (KO) cells (clone D2 used in this study), which have weakened centromeric cohesion [37], were defective in maintaining chromosome bi-orientation and sister-chromatid cohesion during metaphase arrest induced by treatment with the proteasome inhibitor MG132 (Fig 1D and E). These defects were partly rescued by stable overexpression of SFB-Haspin-N469, which is in line with the role of Haspin N-terminus in binding Pds5B and protecting centromeric cohesion [37]. In addition, the inter-kinetochore (inter-KT) distance on chromosome spreads prepared from Haspin-KO cells arrested in mitosis with the spindle microtubule poison nocodazole was 20% further apart than the control, indicative of weakened centromeric cohesion. Compared to full-length SFB-Haspin, SFB-Haspin-N469 was impaired in restoring proper inter-KT distance in Haspin-KO cells (Fig 1F). Thus, even overexpressed Haspin N-terminus is still deficient in supporting centromeric cohesion to the full extent, suggesting a role for Haspin-KD in cohesion protection.

Interaction with Pds5B through the N-terminal PIM of Haspin is required for its centromere localization and centromeric cohesion protection in mitosis (Fig EV1C and D) [37,38]. We next examined the strength of centromeric cohesion when Haspin-KD (residues 471–798) was artificially targeted to centromeres as a fusion protein with the centromere-targeting domain of CENP-B (CB-Haspin-KD-GFP). In nocodazole-arrested mitotic Haspin-KO cells, expression of CB-Haspin-KD-GFP was able to shorten the inter-KT distance by 17.4% (Fig 1G and H). As a positive control, expression of the N-terminus (residues 1–50) of Haspin as a CENP-B fusion protein (CB-Haspin-N50-GFP), but not Haspin-N50-GFP alone (Fig EV1E

and F), also shortened the inter-KT distance as we previously showed [37]. Moreover, CB-Haspin-KD-GFP partly rescued the defects of Haspin-KO cells in maintaining metaphase chromosome bi-orientation and sister-chromatid cohesion during prolonged MG132 treatment (Fig 1I and J). We noticed that the overall centromeric H3pT3 in mitotic Haspin-KO cells expressing CB-Haspin-KD-GFP was 5.8-fold lower than that in control HeLa cells (Fig EV1G), suggesting that artificial targeting of Haspin-KD to centromeres is not sufficient to fully rescue H3pT3. Thus, forced targeting Haspin-KD to the centromere can at least partly bypass the requirement for Pds5B–Haspin interaction in protecting centromeric cohesion.

Taken together, these data indicate the contribution of Haspin-KD to Wapl inhibition and centromeric cohesion protection in mitosis (Appendix Fig S1).

Haspin-KD directly binds the N-terminus of Wapl at the YSR motif

We then set out to investigate how Haspin-KD promotes centromeric cohesion protection. We detected reciprocal co-immunoprecipitation (co-IP) of stably expressed SFB-Haspin with endogenous Wapl from nocodazole-arrested mitotic HeLa cell lysates, but not from interphase cell lysates (Fig 2A and B). Using recombinant H3 (residues 1–45) fused to GST (H3-GST) as the substrate, we detected H3-T3 phosphorylation by endogenous Wapl immunoprecipitates from mitotic HeLa cells, but not from Haspin-KO cells (Fig 2C and D), indicating the specific association between the endogenous proteins of Haspin and Wapl in mitotic cells. Furthermore, GST-fused Wapl (residues 1–33) (GST-Wapl-N) specifically pulled down SFB-Haspin from mitotic cell lysates (Fig 2E). In addition, Wapl (residues 1–28) fused to GST (Wapl-N-GST) efficiently pulled down bacterially expressed and purified recombinant 6xHis-Haspin-KD (residues 471–798) (Fig 2F). Thus, the YSR motif-containing N-terminal short fragment of Wapl is sufficient to bind Haspin-KD directly.

We noticed that Wapl-N-GST and H3-GST pulled down 6xHis-Haspin-KD with comparable efficiency (Fig 2F and G) and that the amino acid sequence of highly conserved very N-terminus of Wapl and histone H3 showed some similarity (Fig EV2A). Previous studies reported the structure of Haspin-KD [50,51], and the co-crystal structure of Haspin-KD with histone H3 peptide ARTK₄Q [Protein Data Bank (PDB): 4OUC] [52], which enabled us to build a model of Haspin-KD in complex with the Wapl peptide GKTY₉ (Fig 2H). The model predicted multiple interactions between the residues of Wapl and Haspin. In particular, similar to the H3-K4 in binding Haspin-KD [39,52], Y9 of Wapl was predicted to form hydrogen bonds with D707 and D709 of Haspin. Indeed, the Wapl-N-Y9A-GST mutant was deficient in binding 6xHis-Haspin-KD in the pulldown assay (Fig 2I). Moreover, 6xHis-Haspin-KD-D707L/D709N showed over 50% reduction in the binding affinity for Wapl (Figs 2J and EV2B–D), as well as H3-GST (Fig EV2E) [51]. These data demonstrate the importance of residues D707 and D709 of Haspin for binding the YSR motif of Wapl *in vitro*.

Taken together, we conclude that Haspin-KD directly binds the flexible N-terminus of Wapl at the YSR motif, akin to its interaction with the N-terminal tail of histone H3.

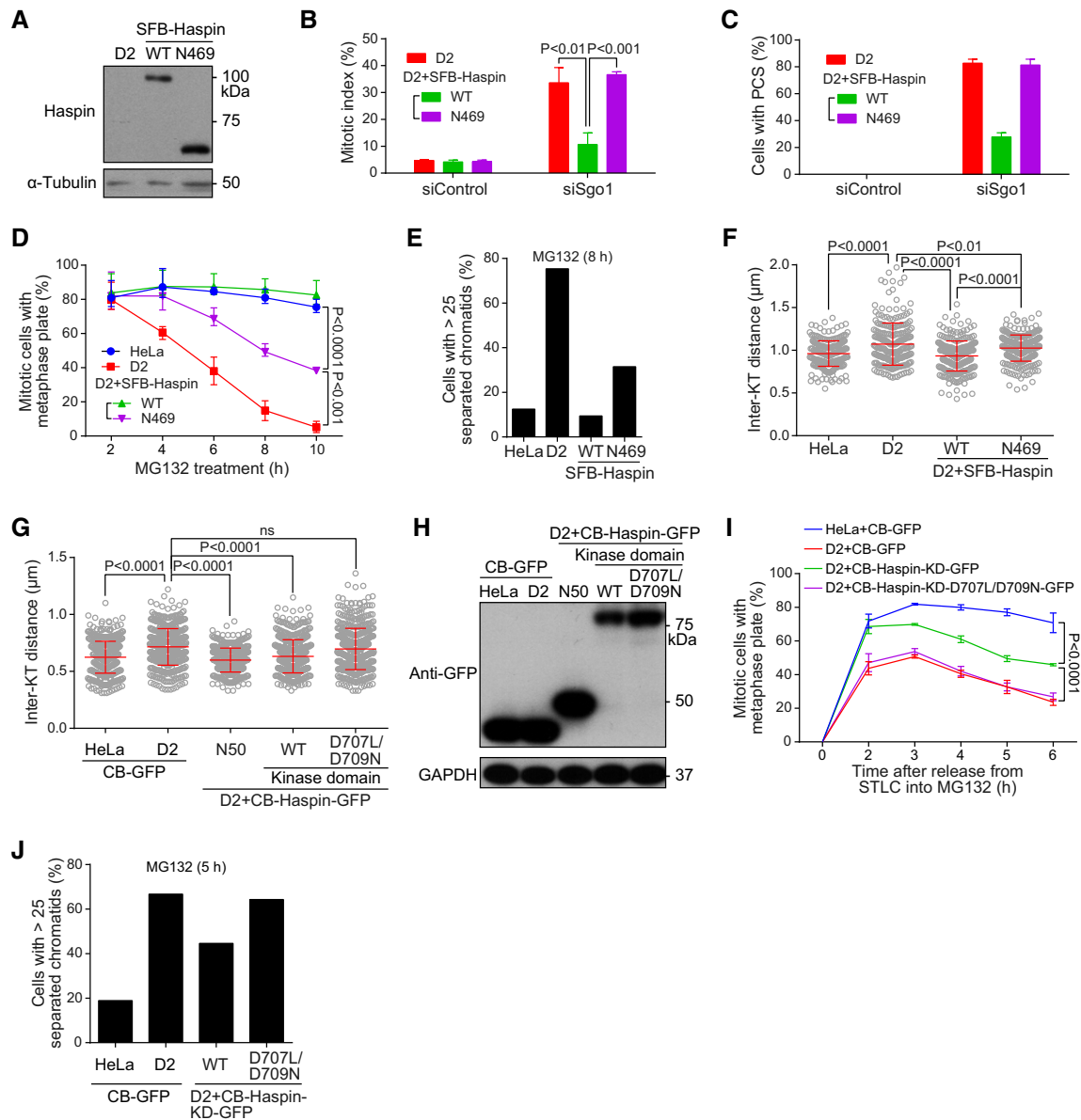


Figure 1. Haspin-KD contributes to Wapl inhibition and centromeric cohesion protection in mitosis.

- A** Lysates of asynchronous Haspin-KO clone D2 cells, with or without stable overexpression of SFB-Haspin (WT or N469), were immunoblotted. See also Fig EV1A.
- B** The indicated cell lines were transfected with control or Sgo1 siRNA. After 36 h, the mitotic index, defined as the percentage of cells in prophase, prometaphase, and metaphase, was quantified in over 3,000 cells ($n = 3$, unpaired *t*-test).
- C** Cells treated as in (B) were exposed to nocodazole for 3 h. Mitotic chromosome spreads were immunostained (see Fig EV1B). The percentage of cells with PCS, defined as at least 26 separated chromatids per cell, was determined in over 160 cells. Means and ranges are shown ($n = 2$).
- D** The indicated cell lines were exposed to MG132, then fixed at the indicated time points to stain DNA. The percentage of mitotic cells with near-standard metaphase plate (< 3 misaligned chromosomes) was determined in over 300 cells ($n = 3$, two-way ANOVA).
- E** Cells were exposed to MG132 for 8 h. Using mitotic chromosome spreads, the percentage of cells with PCS was determined in over 70 cells.
- F** Cells were treated with nocodazole for 3 h. Mitotic chromosome spreads were stained with CENP-C antibodies and DAPI. The inter-KT distance was measured on over 300 chromosomes in over 10 cells (unpaired *t*-test).
- G, H** HeLa and Haspin-KO cells transiently expressing the indicated CENP-B fusion proteins were exposed to nocodazole for 3 h; then, mitotic cells were cytospun onto coverslips, fixed, and stained with H3pT3 or CENP-C antibodies and DAPI. Example images are shown in Fig EV1G. The inter-KT distance was measured on over 500 chromosomes in 20 cells (G, unpaired *t*-test). Asynchronous cell lysates were analyzed by immunoblotting (H).
- I** HeLa- and Haspin-KO cells transiently expressing the indicated CENP-B fusion proteins were released from 8-h treatment with STLCL into MG132, then fixed at the indicated time points for staining with H3pT3 or CENP-C antibodies and DAPI. The percentage of mitotic cells with near-standard metaphase plate was determined in over 300 cells ($n = 3$, two-way ANOVA).
- J** Cells were treated as in (I). At 5 h after STLCL washout, mitotic cells were collected to prepare chromosome spreads; then, the percentage of cells with PCS was determined in over 50 cells.

Data information: Means and SDs are shown (B, D, F, G, and I). See also Fig EV1.

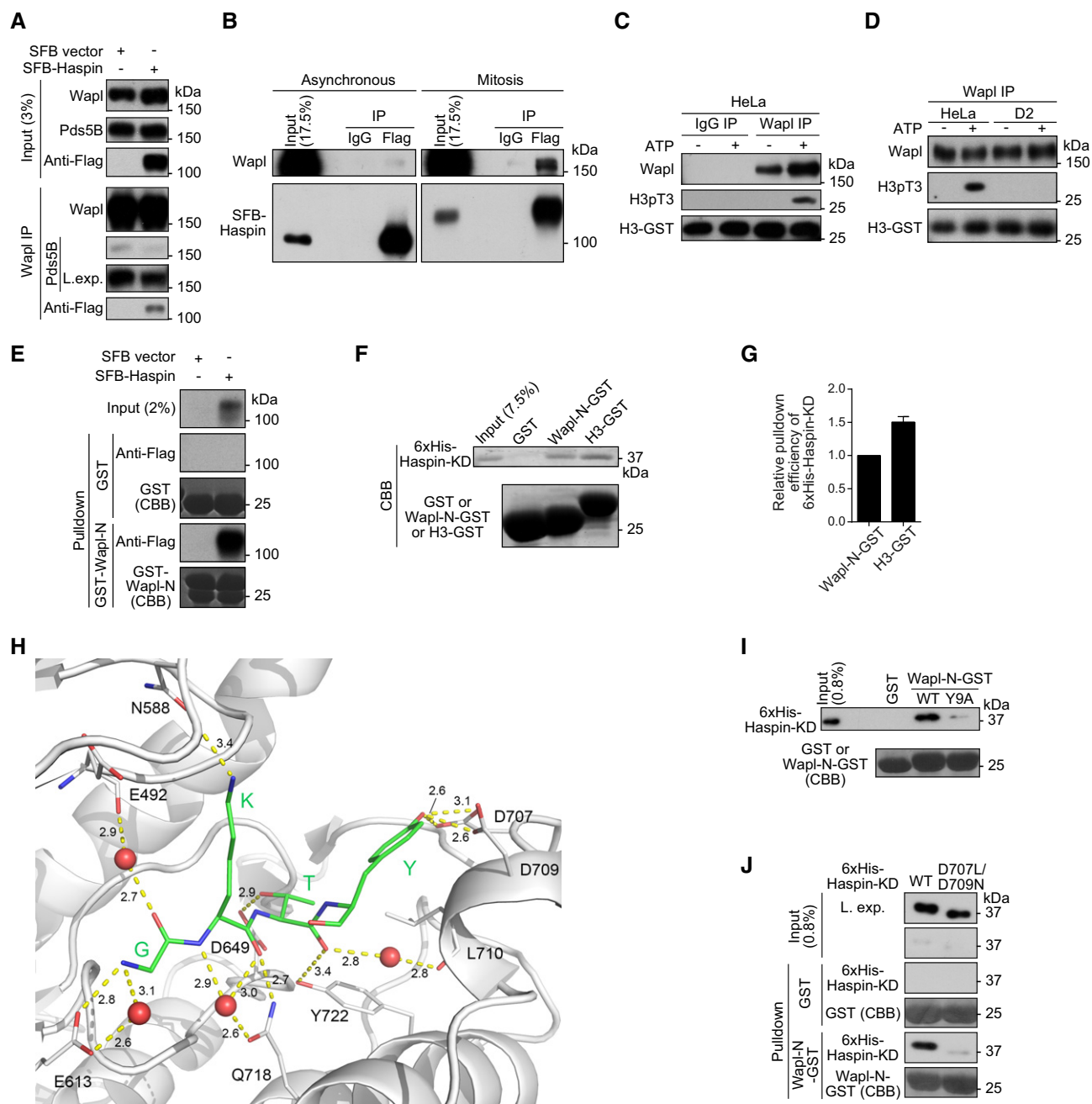


Figure 2. Haspin-KD directly binds the N-terminus of Wapl at the YSR motif.

- A Lysates of nocodazole-arrested mitotic HeLa cells with or without stable expression of SFB-Haspin were subjected to immunoprecipitation followed by immunoblotting with the indicated antibodies.
- B Lysates of asynchronous or nocodazole-arrested mitotic HeLa cells stably expressing SFB-Haspin were subjected to immunoprecipitation with the Flag antibody or control IgG, followed by immunoblotting with antibodies for Wapl or Flag.
- C, D H3-GST was subjected to phosphorylation by endogenous Wapl immunoprecipitates from nocodazole-arrested mitotic HeLa- or Haspin-KO cells, and analyzed by immunoblotting.
- E Lysates of nocodazole-arrested mitotic Haspin-KO cells with or without expression of SFB-Haspin were subjected to pull-down by GST or GST-Wapl-N, followed by anti-Flag immunoblotting or CBB staining for GST proteins.
- F, G 6xHis-Haspin-KD was subjected to pull-down by GST, Wapl-N-GST, or H3-GST followed by CBB staining (F). The relative pull-down efficiency was determined (G). Means and ranges are shown ($n = 2$).
- H The model of Haspin in complex with the Wapl peptide GKYT₉. Haspin is shown in gray cartoon. The bound Wapl peptide is shown in green stick representation. Nitrogen and oxygen atoms are shown in blue and red, respectively. Water molecules are shown as red spheres. Dashes represent probable interactions. Marked residues of Haspin which may interact with the Wapl peptide are represented with gray sticks.
- I 6xHis-Haspin-KD was subjected to pull-down by GST or Wapl-N-GST (WT or Y9A), followed by anti-6xHis immunoblotting or CBB staining.
- J 6xHis-Haspin-KD (WT or D707L/D709N) was subjected to pull-down by GST or Wapl-N-GST and analyzed as in (I).

Data information: L. exp., long exposure. See also Fig EV2.

The binding of Haspin to Wapl displaces Pds5B from Wapl *in vitro*

Given the common requirement for the YSR motif of Wapl in binding Haspin-KD and Pds5B (Figs 2I and EV3A) [11], we speculated that the binding of Haspin-KD and Pds5B to Wapl-YSR is competitive. To test this possibility, Wapl-N-GST was used to bind increasing concentrations of 6xHis-Haspin-KD and was subsequently subjected to pull down MBP-Pds5B-N (residues 1–300). We found that Wapl-N-GST pre-bound by 6xHis-Haspin-KD was deficient in binding MBP-Pds5B-N (Fig 3A). Moreover, simultaneous addition of 6xHis-Haspin-KD reduced the capability of Wapl-N-GST to pull down recombinant MBP-Pds5B-N (Fig 3B), as well as endogenous Pds5B in cell lysates (Fig 3C).

In multiple Wapl-N-GST pulldown assays, while the pulldown of Haspin-KD was readily detected by Coomassie Brilliant Blue (CBB) staining, the pulldown of Pds5B-N was only detectable by immunoblotting, suggesting the difference in their binding affinity to Wapl. Indeed, when compared side-by-side with MBP-Pds5B-N, MBP-Haspin-KD (Fig 3D and E) and 6xHis-Haspin-KD (Fig EV3B) were much more efficiently pulled down by Wapl-N-GST. These data suggested that Haspin-KD might dominate over Pds5B in the competition for binding Wapl *in vitro*. Indeed, MBP-Pds5B-N pre-bound to Wapl-N-GST was readily dissociated from Wapl by the addition of 6xHis-Haspin-KD (Fig 3F), whereas 6xHis-Haspin-KD pre-bound to Wapl-N-GST was hardly eluted when subsequently incubated with various doses of MBP-Pds5B-N (Fig 3G). Similarly, simultaneous addition of 6xHis-Haspin-KD substantially reduced the pulldown of MBP-Pds5B-N by Wapl-N-GST in a dose-dependent manner (Fig EV3C), but not vice versa (Fig EV3D). Thus, Haspin-KD binds Wapl-YSR more tightly than Pds5B does, which can displace Pds5B from Wapl *in vitro*.

Haspin phosphorylates Wapl at the YSR motif to inhibit the Wapl–Pds5B interaction

The Haspin–Wapl interaction also prompted us to test whether Wapl is a substrate of Haspin kinase. The structural model of Haspin-KD in complex with the Wapl peptide GKT₈YSRK predicted that Haspin can phosphorylate Wapl at T8 (Fig EV4A). The residues surrounding T8 also match the minimal Haspin substrate consensus of R/K-T-K/Y, which is also preferentially in the N-terminus [52,53]. Indeed, using phospho-specific antibodies for Wapl-T8 phosphorylation (Wapl-pT8), we found that 6xHis-Haspin-KD readily phosphorylated recombinant GST-Wapl-N (Fig 4A), and full-length Myc-Wapl immunoprecipitated from asynchronous cells (Fig 4B), but not the Wapl-T8A mutant, although GST-Wapl-N-T8A efficiently bound to 6xHis-Haspin-KD (Fig EV4B). Consistent with the impaired binding of Haspin-D707L/D709N to Wapl, the D707L/D709N mutant of MBP-Haspin-KD (Fig 4C), and full-length SFB-Haspin immunoprecipitated from mitotic cells (Fig 4D), was largely deficient in phosphorylating Wapl-T8. Thus, Haspin can phosphorylate Wapl-YSR at T8 *in vitro*.

The crystal structure of Pds5B in complex with the Wapl peptide KT₈YSR suggested that phosphorylation at T8 may compromise Wapl binding to Pds5B (Fig EV4C) [11]. The isothermal titration calorimetry (ITC) assay showed that MBP-Pds5B-N bound to Wapl-N (residues 1–28) peptide with a dissociation constant (K_d) of 6.0 μ M (Fig 4E), whereas interaction between MBP-Pds5B-N and

the T8 phosphorylated Wapl-N peptide was undetectable (Fig 4F). Consistently, the phospho-Wapl-N peptide could hardly pull down MBP-Pds5B-N (Fig 4G and H). Furthermore, upon pre-phosphorylation by 6xHis-Haspin-KD, Wapl-N-GST and Wapl-N peptides were defective in binding MBP-Pds5B-N (Figs 4I and EV4D). Thus, Haspin-mediated phosphorylation of Wapl-YSR directly inhibits the Wapl–Pds5B interaction *in vitro*. Besides, compared to the unphosphorylated peptide, the phospho-Wapl-N peptide pulled down 6xHis-Haspin-KD with a 75% reduction of efficiency (Fig EV4E and F), indicating that phosphorylation of Wapl-YSR also reduces its binding affinity for Haspin. This is reminiscent of the decreased binding of Haspin-KD to T3 phosphorylated histone H3 relative to the non-phosphorylated H3 [51], and is in line with Wapl being a substrate of Haspin.

We next examined the effect of phospho-mimetic mutations in the YSR motif on Wapl activity in binding Pds5B and releasing cohesin. As expected, the phospho-mimetic T8E mutant of Wapl-N-GST was largely deficient in pulling down MBP-Pds5B-N (Fig 4J). Tethering Lac-repressor-fused Pds5B residues 1–300 (LacI-Pds5B-N) to the stably integrated LacO repeats recruited WT and the T8V mutant of Myc-Wapl with the latter being less efficiently, but not the Myc-Wapl-T8E mutant, in U2OS cells (Fig EV4G and H). We then depleted endogenous Wapl in HeLa cells with siRNA, complemented them with siRNA-resistant exogenous Wapl, and examined the morphology of chromosome spreads prepared from nocodazole-arrested mitotic cells. Wapl depletion hindered sister-chromatid resolution due to defective cohesin removal through the prophase pathway [7,8]. As previously reported [5,30], expression of Wapl-GFP restored sister-chromatid resolution in endogenous Wapl-depleted cells. However, Wapl-T8E-GFP, as well as the known Pds5-binding-deficient Wapl-Y9A/R11E-GFP mutant [11], was defective in doing so (Figs 4K and L, and EV4I). Similar defect in restoring mitotic sister-chromatid resolution was observed for the Myc-Wapl-T8E mutant (Fig EV4J and K). Thus, phospho-mimetic mutation in the Wapl-YSR motif, which abrogates the Wapl–Pds5 interaction, prevents Wapl from releasing cohesin in cells.

Using Wapl-pT8-specific antibodies, we were not able to reliably detect Wapl-T8 phosphorylation in nocodazole-arrested mitotic HeLa cells. Since modification-specific antibodies are highly influenced by neighboring post-translational modifications (PTMs) [54], the presence of additional PTMs at the Wapl-YSR motif, such as acetylation of K7 [55], may interfere with the antibody recognition for Wapl-pT8. In addition, given the role of Wapl in releasing the majority of cohesin from chromosome arms in prophase, presumably only a small population of Wapl can undergo transient and dynamic phosphorylation at T8, which may be under the detection limitation of our antibodies. Besides, due to the presence of nearby residues of arginine and lysine, our mass spectrometry analysis did not recover the peptides containing Wapl-T8. Given these reasons, our failure in detecting Wapl-pT8 in cells should not be taken as the proof that Haspin-mediated phosphorylation of Wapl-YSR does not occur during mitosis.

A Wapl-binding-deficient mutant of Haspin is defective in protecting mitotic centromere cohesion

To examine the functional importance of Haspin–Wapl interaction for centromeric cohesion protection, we stably expressed Haspin-GFP

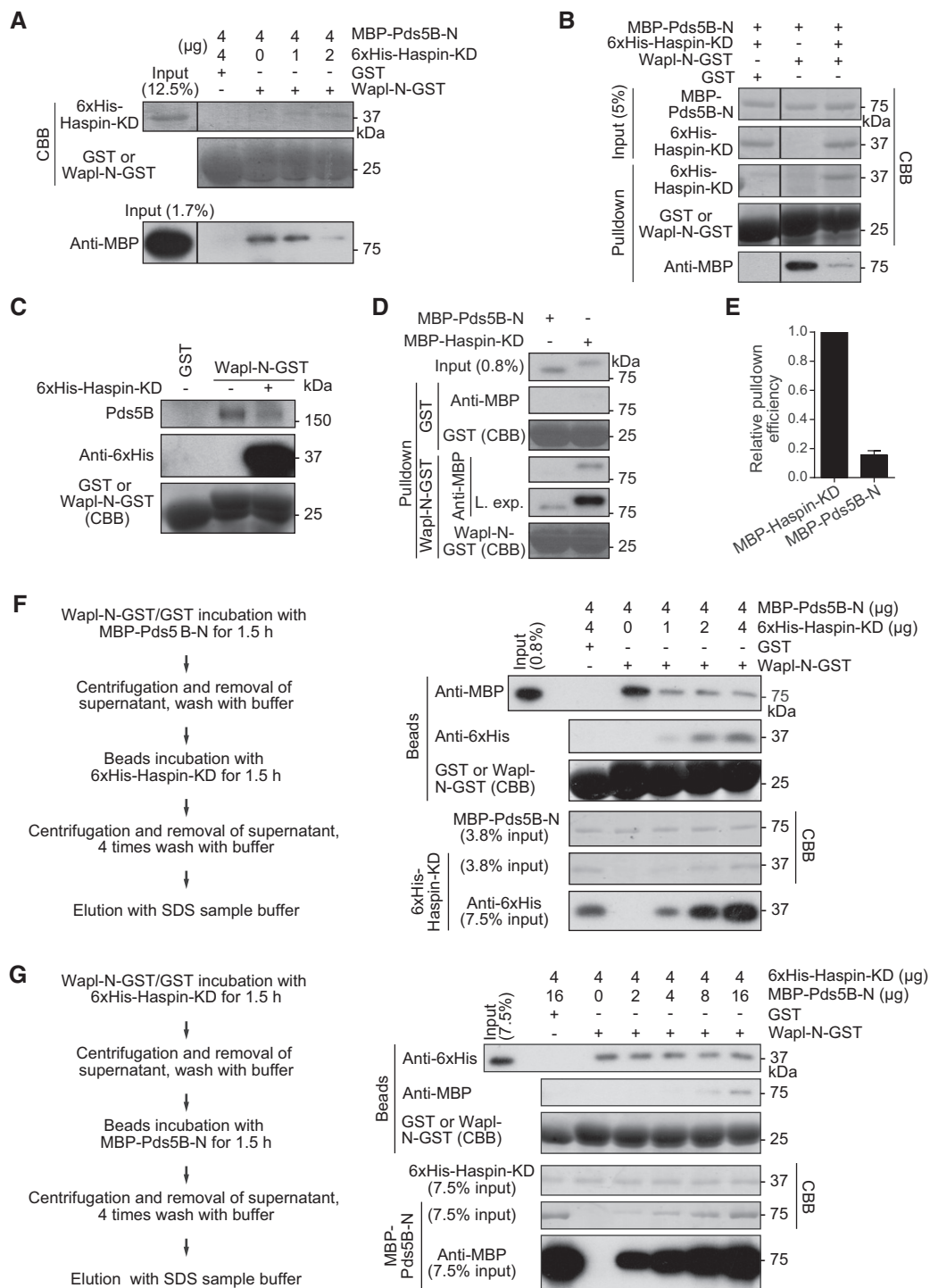


Figure 3. The binding of Haspin to Wapl displaces Pds5B from Wapl *in vitro*.

- A Various amounts of 6xHis-Haspin-KD were subjected to pull-down by GST or Wapl-N-GST. Then, the bead-immobilized GST proteins were washed and subsequently used to pull down MBP-Pds5B-N.
- B MBP-Pds5B-N was subjected to pull-down by GST or Wapl-N-GST in the absence or presence of 6xHis-Haspin-KD.
- C Asynchronous HeLa cell lysates were subjected to pull-down by Wapl-N-GST, in the absence or presence of recombinant 6xHis-Haspin-KD.
- D, E MBP-Pds5B-N or MBP-Haspin-KD was subjected to pull-down by GST or Wapl-N-GST (D). The relative pull-down efficiency was determined (E). Means and ranges are shown ($n = 2$). L. exp., long exposure.
- F MBP-Pds5B-N pre-bound to Wapl-N-GST was incubated with various amounts of 6xHis-Haspin-KD.
- G 6xHis-Haspin-KD pre-bound to Wapl-N-GST was incubated with various amounts of MBP-Pds5B-N.

Data information: All the pull-downs were analyzed by immunoblotting or CBB staining as indicated. See also Fig EV3.

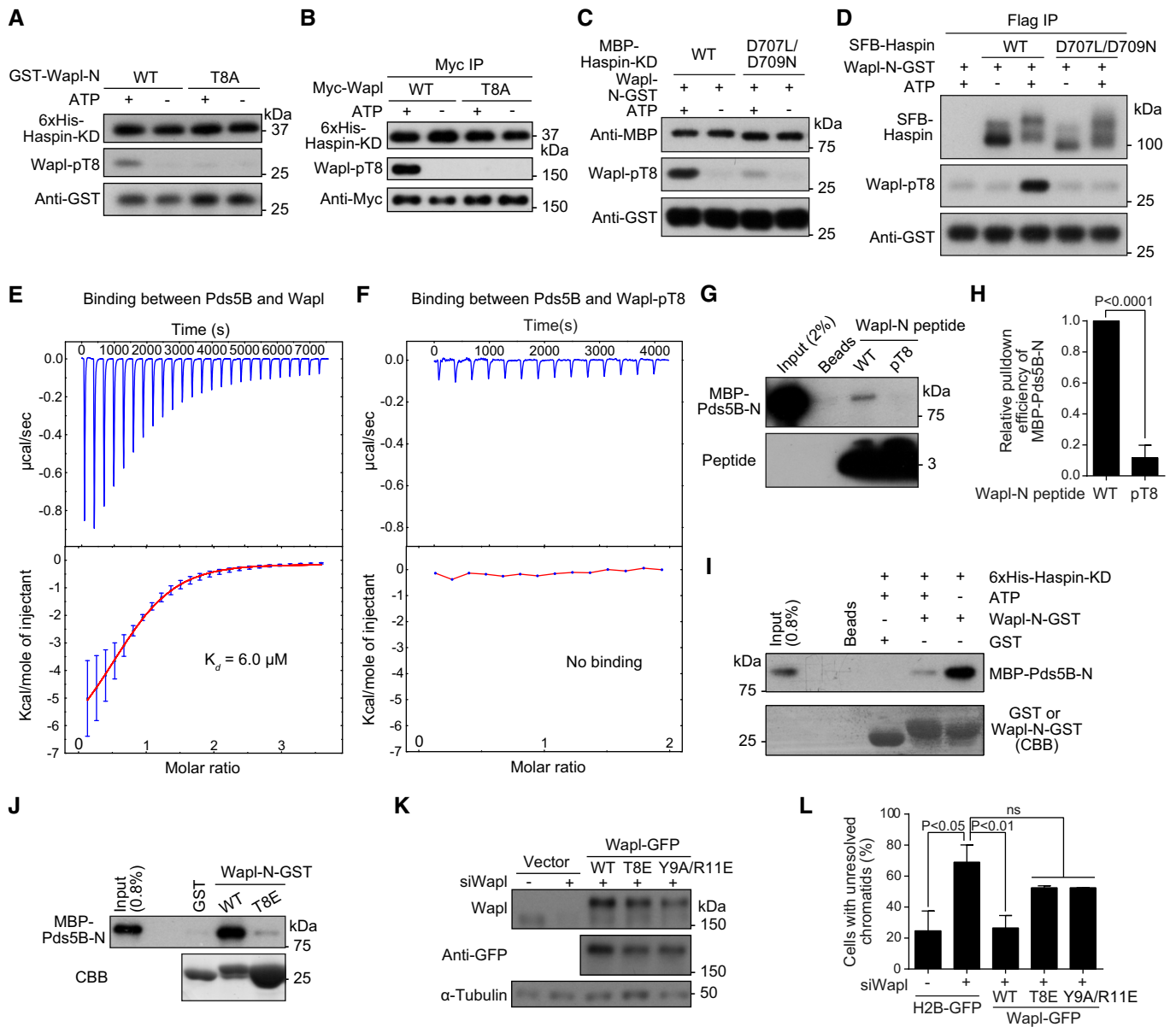


Figure 4. Haspin phosphorylates Wapl at the YSR motif to inhibit the Wapl–Pds5B interaction.

A, B GST-Wapl-N (A), or transiently expressed Myc-Wapl immunoprecipitated from asynchronous cells (B), was subjected to *in vitro* kinase reaction with 6xHis-Haspin-KD, followed by immunoblotting with antibodies to 6xHis, Myc, Wapl-pT8, or GST.

C, D Wapl-N-GST was subjected to *in vitro* kinase reaction with MBP-Haspin-KD (C), or transiently expressed SFB-Haspin immunoprecipitated from mitotic cells (D), followed by immunoblotting with antibodies to Flag, MBP, Wapl-pT8, or GST.

E, F ITC curves of the binding of MBP-Pds5B-N to WT or phospho-Wapl-N peptide. K_d is shown ($n = 3$).

G, H MBP-Pds5B-N was subjected to pulldown by biotinylated Wapl-N (WT or pT8) peptide immobilized on Neutravidin resin, followed by immunoblotting with MBP antibodies or streptavidin-HRP (G). The relative pulldown efficiency was quantified (H; $n = 3$, unpaired *t*-test).

I Wapl-N-GST was subjected to *in vitro* kinase reaction with 6xHis-Haspin-KD. After stringent salt wash, bead-immobilized GST proteins were used to pull down MBP-Pds5B-N, followed by anti-MBP immunoblotting or CBB staining.

J MBP-Pds5B-N was subjected to pulldown by GST or Wapl-N-GST (WT or T8E) followed by anti-MBP immunoblotting or CBB staining.

K, L HeLa cells were transfected with the indicated siRNAs and plasmids, then were lysed for immunoblotting (K), or treated with nocodazole for 3 h to prepare chromosome spreads for immunostaining (see Fig EV4). The percentages of mitotic cells with sister chromatids unresolved were quantified (L; $n = 3$, unpaired *t*-test).

Data information: Means and SDs are shown (E, H and L). See also Fig EV4.

(WT or the Wapl-binding-deficient D707L/D709N mutant) in Haspin-KO cells (Fig EV5A). Immunofluorescence microscopy of chromosome spreads prepared from nocodazole-arrested mitotic

cells showed that both WT and the D707L/D709N mutant of Haspin-GFP mainly localized to the mitotic centromeres (Fig 5A), though the mutant was 2.3-fold less concentrated than the WT protein

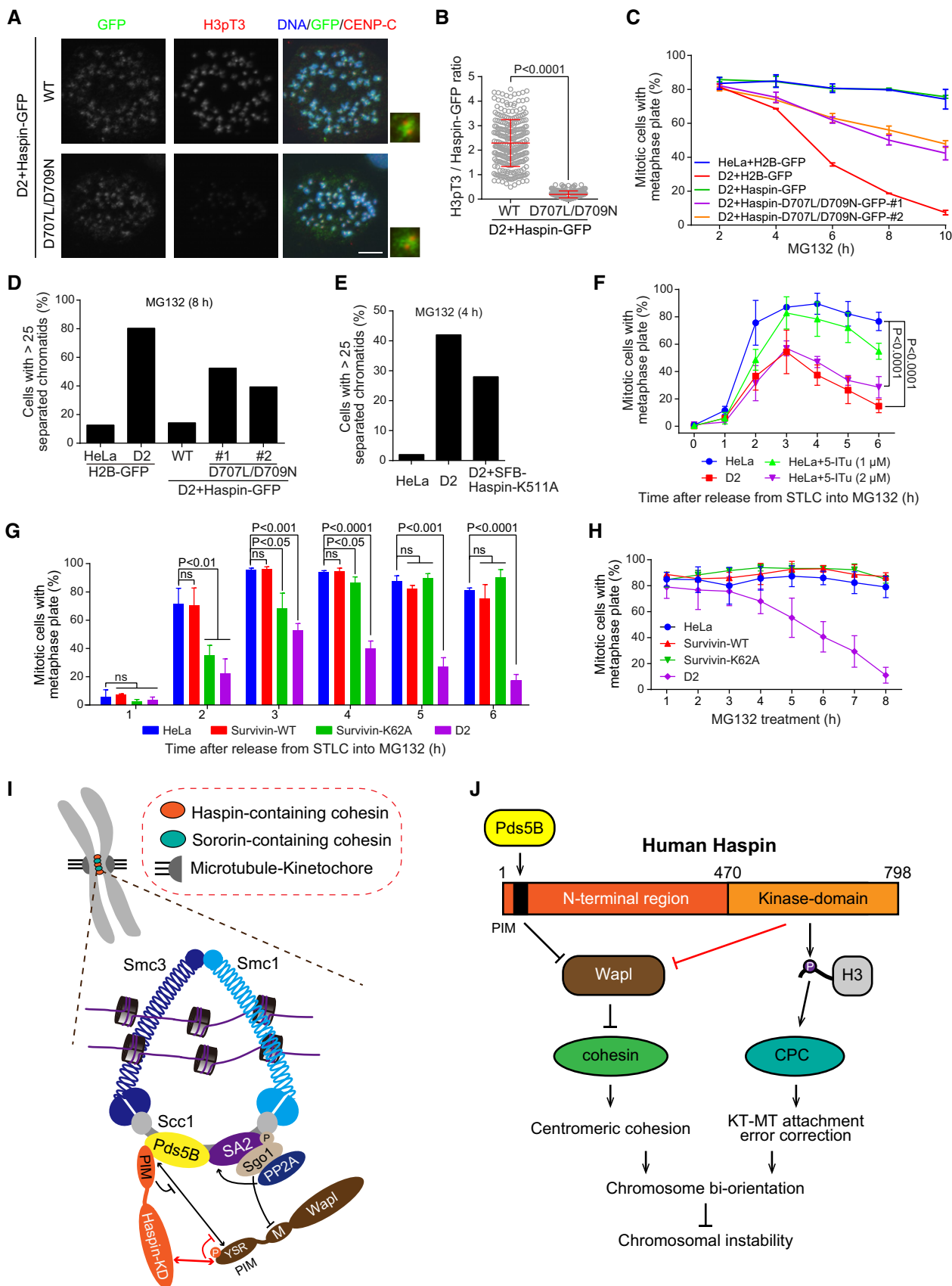


Figure 5.

Figure 5. The Haspin–Wapl interaction and Haspin kinase activity are required for the protection of mitotic centromere cohesion.

- A, B Haspin-KO cells stably overexpressing Haspin-GFP or Haspin-D707L/D709N-GFP (clone #2) were exposed to nocodazole for 3 h. Mitotic chromosome spreads were immunostained with antibodies for anti-GFP, H3pT3, or CENP-C. Example images are shown (A). The centromeric H3pT3/Haspin-GFP immunofluorescence intensity ratio was determined on over 500 chromosomes in 20 cells (B, $n = 3$, unpaired *t*-test).
- C The indicated stable cell lines were exposed to MG132, fixed at the indicated time points, and then stained with GFP antibodies and DAPI. The percentage of mitotic cells with near-standard metaphase plate was determined in over 200 cells. Means and ranges are shown ($n = 2$).
- D The indicated cell lines were exposed to MG132 for 8 h. Using mitotic chromosome spreads (see Fig EV5E), the percentage of cells with PCS was determined in over 60 cells.
- E HeLa- and Haspin-KO cells with or without stable overexpression of SFB-Haspin-K511A were exposed to MG132 for 4 h. Using mitotic chromosome spreads, the percentage of cells with PCS was determined in 72 cells for each condition.
- F HeLa and clone D2 cells were released from 3-h treatment with STLC into MG132-containing medium, in the absence or presence of Haspin inhibitors, and then fixed at the indicated time points for DNA staining. The percentage of mitotic cells with near-standard metaphase plate was determined in around 300 cells ($n = 3$, two-way ANOVA).
- G The indicated cell lines were released from 5-h treatment with STLC into MG132-containing medium and then fixed at the indicated time points for DNA staining. The percentage of mitotic cells with near-standard metaphase plate was determined in around 300 cells ($n = 3$, unpaired *t*-test).
- H The indicated cell lines were exposed to MG132 and then fixed at the indicated time points to stain DNA. The percentage of mitotic cells with near-standard metaphase plate was determined in around 300 cells ($n = 3$).
- I A schematic of Haspin-containing centromeric cohesin complex. Double-headed arrows represent interactions.
- J Schematic depiction of the role for Haspin in ensuring chromosome bi-orientation during mitosis.
- Data information: Means and SDs are shown (B, F–H). Scale bars, 10 μm . See also Fig EV5.

(Fig EV5B). Moreover, compared to Haspin-GFP, Haspin-D707L/D709N-GFP generated 11.8-fold less H3pT3 at centromeres (Fig 5B). This is consistent with the impaired binding of 6xHis-Haspin-KD-D707L/D709N to histone H3 (Fig EV2B–D), as well as the markedly decreased H3-T3 phosphorylation by this mutant *in vitro* [51].

Haspin-KO cells showed increased distance between sister kinetochores as we previously showed [37], which was efficiently restored by Haspin-GFP (Fig EV5C and D). However, Haspin-D707L/D709N-GFP expressed at the levels comparable to those of Haspin-GFP was deficient in supporting proper inter-KT distances. Moreover, during MG132-induced metaphase arrest, the Haspin-D707L/D709N-GFP mutant was not able to rescue the defects in maintaining chromosome bi-orientation (Fig 5C) and sister-chromatid cohesion (Figs 5D and EV5E) to the same extent as similar levels of Haspin-GFP did. These results indicate that cells expressing the D707L/D709N mutant of Haspin have weakened centromeric cohesion. This may explain the moderately reduced localization of Haspin-D707L/D709N-GFP at mitotic centromeres, given that centromeric recruitment of Haspin requires its interaction with Pds5B and that Pds5B requires cohesin to localize at centromeres [37,38,40,46]. Thus, even when overexpressed, the Haspin-D707L/D709N-GFP mutant only partly rescues the centromeric cohesion defects in Haspin-KO cells. In addition, CENP-B-fused Haspin-KD-D707L/D709N-GFP was defective in supporting proper inter-KT distance, metaphase chromosome bi-orientation, and sister-chromatid cohesion in Haspin-KO cells (Fig 1G–J).

Taken together, these data demonstrate that interaction with Wapl is required for Haspin to support strong cohesion at mitotic centromeres. However, the cohesion defects in cells expressing the Haspin-D707L/D709N mutant did not allow us to distinguish whether this is due to reduced Wapl-YSR phosphorylation and/or due to the reduced affinity for Wapl that makes Haspin a poor competitor for Pds5B.

Haspin kinase activity promotes centromeric cohesion independently of the H3pT3–Survivin interaction

We recently showed that, even when stably overexpressed (Fig EV5F), the catalytically inactive mutant of Haspin (SFB-Haspin-K511A) only

partly restored the capability of Haspin-KO cells in maintaining metaphase chromosome bi-orientation [37]. Consistently, SFB-Haspin-K511A was impaired in supporting strong sister-chromatid cohesion during metaphase arrest (Fig 5E), as well as proper inter-KT distance in nocodazole-arrested mitotic cells (Fig EV5G). Since Wapl-N-GST was deficient in pulling down 6xHis-Haspin-KD-K511A (Fig EV5H), the centromeric cohesion defects in cells overexpressing SFB-Haspin-KD-K511A could not be unequivocally attributed to the potential contribution of Haspin kinase activity to cohesion protection, similar to the Haspin-D707L/D709N mutant.

We thus investigated whether chemical inhibition of Haspin kinase activity in mitosis compromises centromeric cohesion. When nocodazole-arrested mitotic HeLa cells were treated for 1 h with various small-molecule inhibitors of Haspin, the inter-KT distances on mitotic chromosome spreads were 11–15% further apart than the control (Fig EV5I and J), indicative of weakened centromeric cohesion. We next examined metaphase chromosome bi-orientation when cells were released from STLC into MG132 in the absence or presence of Haspin inhibitors. As expected, treatment with the Haspin inhibitor 5-ITu delayed the metaphase chromosome bi-orientation (Fig 5F), reflecting the role of H3pT3-dependent CPC in correcting erroneous kinetochore–microtubule (KT-MT) attachments [40–42]. Importantly, Haspin inhibitor-treated cells were defective in maintaining chromosome bi-orientation on the metaphase plate during the sustained metaphase arrest, consistent with the centromeric cohesion defects. In addition, the pulldown of 6xHis-Haspin-KD by Wapl-N-GST was not affected by 5-ITu up to 20 μM (Fig EV5K), suggesting that treatment of mitotic cells with Haspin inhibitors may not compromise the interaction of Haspin-KD with Wapl. These data strongly suggest that Haspin kinase activity, likely toward Wapl, is the main contributor to centromeric cohesion protection.

The contribution of Haspin kinase activity to the maintenance of mitotic centromere cohesion is in stark contrast to the role of mitotic kinases Plk1, Cdk1, and Aurora B in promoting cohesin release from chromosome arms through phosphorylating cohesin and its protector Sororin [18,28,31,56–61].

Other than Wapl phosphorylation discovered in this study, the only known readout of Haspin kinase activity in mitosis is H3pT3 [39], which is directly recognized by the Survivin subunit of CPC

[40–42]. It is thus possible that the defect in centromeric cohesion protection described above can also be contributed by CPC mislocalization. We then directly examined whether the H3pT3-dependent recruitment of CPC to centromeres is required for the protection of centromeric cohesion. Using CRISPR/Cas9, we stably depleted endogenous Survivin in HeLa cells stably expressing exogenous Survivin-Myc-6xHis, or the Survivin-K62A-Myc-6xHis mutant lacking phospho-specific interaction with H3pT3 (Fig EV5L and M) [62]. Compared to the control Survivin-WT cells, cells expressing the Survivin-K62A mutant showed 2.9-fold in the centromeric localization of Aurora B, the kinase subunit of CPC (Fig EV5N and O). Consequently, these mutant cells were delayed in chromosome bi-orientation when released from STLC into MG132. However, they were proficient in achieving and maintaining proper alignment of chromosomes on the metaphase plate (Fig 5G). Similar results were obtained in HeLa cells in which endogenous Survivin was stably replaced by the exogenous Survivin-H80A-Myc-6xHis mutant (Fig EV5P) incapable of binding histone H3 and H3pT3 [62–64]. Furthermore, the Survivin-K62A-mutant cells efficiently maintained metaphase chromosome bi-orientation during the prolonged MG132 treatment (Fig 5H) and showed proper inter-KT distances (Fig EV5Q). Thus, loss of H3pT3–Survivin interaction does not cause detectable weakening of centromeric cohesion, though it obviously compromises the efficiency of chromosome bi-orientation. These results indicate that Haspin kinase activity contributes to centromeric cohesion protection independently of the H3pT3-dependent recruitment of CPC to centromeres.

Hengeveld *et al* [65] recently proposed that the CPC is localized at the inner centromere to sustain centromere cohesion on bi-oriented chromosomes. It is possible that another pool of CPC, which is recruited to mitotic centromeres independently of Survivin binding to H3pT3, might contribute to the protection of centromere cohesion during metaphase. Indeed, weak accumulation of CPC at centromeres was still detectable in cells expressing the K62A or H80A mutant of Survivin (Fig EV5N and O). This could be due to the recruitment of CPC by the Shugoshin proteins which bind to histone H2A with T120 phosphorylation (H2ApT120) at mitotic centromeres [33,40,66], or by other unidentified mechanisms.

In sum, these results support the model that Haspin phosphorylates Wapl at the YSR motif to directly inhibit the Wapl–Pds5B interaction. We suggest that the centromeric cohesion defects in cells treated with Haspin inhibitors might be due to decreased phosphorylation of Wapl-YSR. However, we cannot rule out the possibility of additional effects of loss of H3pT3, other than delocalization of H3pT3-dependent centromeric CPC, which would result in cohesion defects. Besides, we cannot fully exclude the possibility that Haspin kinase activity toward another unknown target also contributes to cohesion protection.

Conclusion

Taken together, we propose that there are different pools of centromeric cohesin complexes in which Pds5B binds to either Haspin or Sororin, another Wapl antagonist [11,18,67–69]. The interaction of Pds5B with the N-terminal PIM of Haspin enables the centromeric localization of Haspin, which can competitively interfere with the YSR motif-dependent binding of Wapl to Pds5B. The centromeric

Haspin uses its C-terminal kinase domain to bind and phosphorylate Wapl at the YSR motif, thereby directly inhibiting the Wapl–Pds5B interaction at mitotic centromeres and preventing Wapl-mediated release of the Haspin-containing cohesin complex (Fig 5I). We therefore conclude that Haspin ensures mitotic chromosome bi-orientation not only by promoting the H3pT3-dependent centromeric localization of CPC to correct improper KT-MT attachments, but also by antagonizing Wapl to protect centromeric cohesin (Fig 5J). This study provides new insight into how different factors in the complex centromere signaling network are specialized to meet the multiple challenges encountered on the road to accurate chromosome segregation in mitosis [70].

Materials and Methods

Cell culture, plasmids, siRNA, transfection, and drug treatments

All cells were cultured in DMEM supplemented with 1% penicillin/streptomycin and 10% FBS (Gibco) and maintained at 37°C with 5% CO₂. Cells stably expressing SFB-Haspin proteins were maintained in 0.2 µg/ml puromycin (Calbiochem). Cells stably expressing Haspin-GFP proteins were isolated and maintained in blasticidin (Sigma) at 3 and 1.5 µg/ml, respectively. Cells stably expressing pEF6-Survivin-Myc-His were maintained in 2 µg/ml blasticidin.

The original Haspin cDNA and Myc-Wapl plasmid were kindly provided by Drs Jonathan Higgins (Newcastle University, UK) and Hongtao Yu (University of Texas Southwestern Medical Center, USA), respectively. SFB-Haspin, pBos-CENP-B-GFP, and pBos-CENP-B-Haspin-N50-GFP were previously described [37]. SFB-Haspin-N469 was made by introducing a stop codon at Haspin-K470. pBos-Haspin-GFP and pBos-Wapl-GFP were constructed by replacing the H2B fragment in pBos-H2B-GFP (Clontech) with the KpnI/BamHI-digested PCR fragments encoding full-length Haspin and Wapl, respectively. To make pBos-CENP-B-Haspin-KD-GFP constructs, the PCR fragments encoding Haspin residues 471–798 were subcloned into the BamHI site of pBos-CENP-B-GFP. All point mutations were introduced with the QuikChange II XL site-directed mutagenesis kit (Agilent Technologies). All plasmids were sequenced to verify desired mutations and absence of unintended mutations.

For Wapl RNAi rescue experiments (Figs 4K and L, and EV4I–K), HeLa cells were transfected twice with control or Wapl siRNAs in a 24-h interval. At 4 h after the second siRNA transfection, cells were transfected with the siRNA-resistant Wapl-GFP or Myc-Wapl plasmids. After 24 h, cells were lysed for immunoblotting, or treated with nocodazole for 3 h to prepare chromosome spreads for immunostaining. The following siRNA duplexes were ordered from Integrated DNA Technologies (IDT): siWapl (5′-CGGACUACCCUUA GCACAAdTdT-3′), siSgo1 (5′-CAGUAGAACCUGCUCAGAAAdTdT-3′), and siPds5B (5′-GAGACGACUCUGAUCUUGUdTdT-3′). Plasmid and siRNA transfections were done with Fugene 6 (Promega) and Lipofectamine RNAiMAX (Invitrogen), respectively. Cells were arrested in prometaphase with 0.16–3.3 µM nocodazole (Selleckchem). Drugs used in this study were STLC (5 µM, Tocris Bioscience), MG132 (5–20 µM, Sigma), and 5-iodotubercidin (5-ITu, 1–10 µM, Tocris). LDN-192960 (10 µM) and LDN-211898 (30 µM) were kindly provided by Dr. Jonathan Higgins. Mitotic cells were collected by selective detachment with “shake-off”.

Antibodies

Rabbit polyclonal antibodies used were to H3pT3 (B8633, Dr. Jonathan Higgins), Wapl (A300-268A, Bethyl; for immunoblotting), Cyclin B1 (clone D5C10, Cell Signaling Technology, CST), GFP (A11122, Invitrogen), GST (G7781, Sigma), MBP (E8032, New England BioLabs), GAPDH (14C10, CST), Survivin (NB500-201, Novus Biologicals), Pds5B (A300-537A, Bethyl), and H2ApT120 (Active Motif). Rabbit anti-Wapl-pT8 polyclonal antibodies were produced by immunization with the synthetic phospho-peptide MTSRFGK[pT]YSRKGG. Rabbit anti-Haspin polyclonal antibodies were produced by immunization with the synthetic peptide AADGRRQRRPGREAA, which recognized exogenously expressed Haspin, but not endogenous Haspin. Mouse monoclonal antibodies used were to α -tubulin (T-6047, Sigma), Aurora B (AIM-1; BD Biosciences), 6xHis-tag (GNI4110-HS, GNI), Flag-tag (M2, Sigma), Myc-tag (4A6, Millipore), Wapl (MBL, clone C11-10, code number M221-3; for immunoprecipitation), and H3pT3 (16B2, kindly provided by Dr. Hiroshi Kimura, Osaka University, Japan). Guinea pig polyclonal antibodies against CENP-C were from MBL (PD030). Human centromere autoantibodies were from Immunovision. Secondary antibodies for immunoblotting were goat anti-rabbit or horse anti-mouse IgG-HRP (CST). Streptavidin-HRP was from ThermoFisher (43–4323). Secondary antibodies for immunostaining were donkey anti-rabbit IgG-Alexa Fluor 488 or Cy3 (Jackson ImmunoResearch), anti-mouse IgG-Alexa Fluor 488 or 546 (Invitrogen), anti-human IgG-Alexa Fluor 647 (Jackson ImmunoResearch), and goat anti-guinea pig IgG-Alexa Fluor 647 (Invitrogen).

CRISPR/Cas9-mediated editing of Survivin gene in HeLa cells

Single-guide RNA (sgRNA) for human Survivin gene was ordered as oligonucleotides from IDT, annealed, and cloned into the BbsI site of dual Cas9 and sgRNA expression vector pX330 (Addgene). The plasmids were transfected into HeLa cells stably expressing Survivin-Myc-6xHis using Fugene 6 (Promega). After 48-h incubation, cells were split individually to make a clonal cell line with selection using 1 μ g/ml puromycin for 2–3 days. The sgRNA targeting a sequence (5'-CTGTCCCTTGAGATGGCCG-3') is at the junction of an intron and the beginning of the second exon of Survivin gene. Clones with strong reduction in centromeric Aurora B were isolated by immunostaining and confirmed by immunoblotting.

Fluorescence microscopy and statistical analysis

Cells grown on coverslips were fixed with 2% paraformaldehyde (PFA) in PBS for 10 min followed by extraction with 0.1 or 0.5% Triton X-100 in PBS for 5 min. Mitotic HeLa cells obtained by shake-off were re-attached to glass coverslips by Cytospin at 1,500 rpm for 5 min, pre-extracted for 5 min with 1% Triton X-100 in PHEM (60 mM Pipes, 25 mM Hepes, 10 mM EGTA, and 2 mM MgCl₂, pH 6.9), then fixed with 4% PFA in PHEM for 20 min. In general, to produce chromosome spreads, mitotic cells obtained by selective detachment were incubated in 75 mM KCl for 10 min, re-attached to glass coverslips by Cytospin, then fixed with 2% PFA in PBS for 20 min followed by extraction with 0.1% Triton X-100 in PBS for 5 min. Fixed cells were stained with primary antibodies for 1–2 h and secondary antibodies for 1 h, all with 3% BSA in PBS

with 0.1–0.5% Triton X-100 and at room temperature. DNA was stained for 10 min with DAPI or Hoechst 33342 (0.5 μ g/ml, Thermo Fisher Scientific).

Fluorescence microscopy was carried out at room temperature using a Nikon ECLIPSE Ni microscope with a Plan Apo Fluor 60 \times Oil (NA 1.4) objective lens and a Clara CCD (Andor Technology). The inter-KT distance was measured using the centromere marker CENP-C or ACA on over 25 kinetochores per cell in at least 20 cells from one or two independent experiments. Distance was determined by drawing a line from the outer kinetochore extending to the outer edge of its sister kinetochore. The length of the line was calculated using the imaging software of NIS-Elements BR (Nikon). Quantification of fluorescent intensity was carried out with ImageJ (NIH) using images obtained at identical illumination settings. Briefly, on chromosome spreads, the average pixel intensity of H3pT3, Aurora B, or Haspin-GFP staining at inner centromeres, defined as regions falling within a 9-pixel-diameter circle at paired centromeres, was determined using ImageJ. ACA or CENP-C intensity was determined within a 9-pixel-diameter circle encompassing single centromere dots. After background correction, the ratio of Haspin-GFP/CENP-C, H3pT3/Haspin-GFP, or Aurora B/ACA intensity was calculated for each centromere. The acquired images were processed using Adobe Photoshop and Adobe Illustrator. Statistical analyses were carried out by unpaired *t*-test using GraphPad Prism 6.

Protein expression and purification

Bacterial expression plasmids of H3-GST (in pETGEX-CT) and 6xHis-Haspin-KD (in pET45b+) were kindly provided by Dr. Jonathan Higgins (Newcastle University, UK). MBP-Haspin-KD and MBP-Pds5B-N were constructed by subcloning Haspin residues 471–798 and Pds5B residues 1–300, respectively, into pGEX-MBP-6xHis. Wapl-N-GST was constructed by subcloning Wapl residues 1–28 into the NcoI/SacI sites of pETGEX-CT. GST-Wapl-N was constructed by subcloning Wapl residues 1–33 into pGEX-4T1. The plasmids were transformed into BL21 (DE3)-competent cells (Stratagene). Cells were grown in LB broth under antibiotic selection at 37°C until OD₆₀₀ at 0.6–0.7, and protein expression was induced with 0.1–0.4 mM IPTG at 16°C for 16 h or at 37°C for 4 h. Cells were lysed by sonication in buffer A (50 mM Tris-HCl, pH 8.0, 300 mM NaCl, for MBP-Pds5B-N), buffer B (20 mM Tris-HCl, pH 8.0, 100 mM NaCl, 1 mM EDTA, 1% Triton X-100 or 0.5% NP-40, for GST fusion proteins), or buffer C (40 mM Tris-HCl, 300 mM NaCl, 1% Triton X-100, 20 mM imidazole, pH 7.4, for 6xHis-Haspin-KD). The lysate was clarified by centrifugation and incubated with Amylose Resin (BioLab), glutathione Sepharose 4B (GE Healthcare), or Ni-NTA resin (Qiagen) beads, all in lysis buffer. The resins were washed with lysis buffer and eluted with 10 mM maltose, 10 mM glutathione, or 300 mM imidazole.

Immunoblotting and immunoprecipitation

SDS-PAGE, immunoblotting, and immunoprecipitation were carried out using standard procedures. Cell lysates were prepared in standard SDS sample buffer or Lamond buffer for immunoblotting. For the co-immunoprecipitation (Figs 2A–D and 4D), cells were lysed in P50 buffer containing 25 mM Tris-HCl, pH 7.5, 50 mM NaCl, 0.1% NP-40, 2 mM MgCl₂, 10% glycerol, 1 mM dithiothreitol (DTT),

protease inhibitor cocktail (P8340, Sigma), 1 mM PMSF, 0.1 μ M okadaic acid (Calbiochem), 10 mM NaF, 20 mM β -glycerophosphate, and benzamide hydrochloride (Merck). After the removal of insoluble materials by high-speed centrifugation, lysates were precleared with GammaBind G Sepharose (17-0885-02, GE Healthcare). Lysates were incubated with antibodies for 3 h at 4°C before the addition of GammaBind G Sepharose for a further 1 h. Beads were washed several times with the lysis buffer with 150 mM NaCl, boiled in standard SDS sample buffer, and subject to immunoblotting.

GST pulldown and peptide pulldown

For GST-Wapl-N pulldown of SFB-Haspin (Fig 2E), nocodazole-arrested mitotic HeLa cells stably expressing SFB-Haspin were lysed in P50 buffer with 150 mM NaCl. The lysates were precleared with glutathione Sepharose 4B beads, then incubated with GST fusion proteins immobilized to glutathione Sepharose 4B beads for 2 h. For Wapl-N-GST pulldown of endogenous Pds5B (Fig 3C), asynchronous HeLa cells were lysed in P50 buffer, precleared, then subjected to GST pulldown in the absence or presence of 6xHis-Haspin-KD. For Wapl-N-GST or H3-GST pulldown of 6xHis-Haspin-KD, MBP-Haspin-KD, or MBP-Pds5B-N, these recombinant proteins were incubated for 1 h with bead-immobilized GST fusion proteins in P150 buffer (50 mM Tris-HCl, pH 7.5, 150 mM NaCl, 0.5% Triton X-100). For the data in Fig 2I and J, pulldown was conducted in P150 buffer with 300 mM NaCl. For peptide pulldown of MBP-Pds5B-N (Fig 4G) or 6xHis-Haspin-KD (Fig EV4E), 1 μ g Wapl-N peptides (WT or pT8) was incubated with 4 μ g recombinant proteins in 500 μ l P150 buffer for 4 h, then incubated with NeutrAvidin Plus Ultralink Resin (Thermo Fisher Scientific) for 1 h. The Wapl peptide of residues 1–28 (95% pure) followed by Lys-biotin was synthesized by GL Biochem (Shanghai). Following all these pulldown assays that were conducted at 4°C, the beads were washed 3–5 times with the same buffer and subjected to analysis by immunoblotting or CBB staining.

In vitro kinase reaction

For phosphorylation of GST-Wapl-N, Wapl-N-GST or Wapl-N peptide (Figs 4A, C, I and EV4D), 0.5 μ g substrates was incubated with 0.2 μ g recombinant Haspin-KD. For phosphorylation of Myc-Wapl (Fig 4B), asynchronous HEK293T cells transiently expressing Myc-Wapl were lysed in buffer containing 50 mM Tris-HCl, pH 7.5, 500 mM NaCl, 0.1% NP-40, and 10 mM $MgCl_2$ with protease inhibitors and phosphatase inhibitors as in P50 buffer; then, the anti-Myc immunoprecipitates were subjected to phosphorylation by 0.2 μ g 6xHis-Haspin-KD. The kinase reactions were conducted in 50 μ l kinase reaction buffer (50 mM Tris-HCl pH 8.0, 150 mM NaCl, 10 mM $MgCl_2$) with 0.2 mM ATP for 20 min at 30°C. The reactions were terminated with SDS sample buffer, boiled, and analyzed by immunoblotting.

Isothermal titration calorimetry and fitting

Measurements of the heat exchange associated with MBP-Pds5B-N (residues 1–300) binding to synthetic Wapl-N peptide (residues 1–28) were acquired using a microcalorimeter (VP-ITC, GE Healthcare). All experiments were performed at a constant temperature of

25°C. All solutions were filtered and degassed before each experiment. The sample cell ($V = 1.4301$ ml) was filled with MBP-Pds5B-N (17 μ M) sample in the buffer containing 200 mM NaCl and 20 mM Tris-HCl, pH 8.5, whereas the injector contained the same buffer with synthetic Wapl peptide (270 μ M); 25–30 injections were performed with 10 μ l synthetic peptide injected into sample cell each time. The data were fit to a one-site binding model in the Origin program. A constant background was subtracted. The affinities were reported as K_d in the text and figures.

Structural modeling

The structure of Haspin kinase domain in complex with the Wapl peptide GKTYY (Fig 2H) or GKTYSRK (Fig EV4A) was modeled using WinCoot based on the structure of Haspin kinase domain in complex with the H3 peptide ARTKQ (PDB ID: 4OUC). The structure of Pds5B in complex with the Wapl peptide KpTYSR (Fig EV4C) was modeled using WinCoot based on the structure of Pds5B in complex with the Wapl peptide KTYSR (PDB ID: 5HDT). The geometries of the modeled structure were refined using REFMAC. All the figures were made by PyMOL (www.pymol.org).

Expanded View for this article is available online.

Acknowledgements

We thank Drs Xiangwei He and Jonathan Higgins for critically reading the manuscript, and Drs David Spector and Hongtao Yu for kindly providing reagents. This work was supported by grants to FW from National Key Research and Development Program of China (2017YFA0503600), the National Natural Science Foundation of China (NSFC) (31371359, 31571393, 31322032, 31561130155 and 31771499), the Natural Science Foundation of Zhejiang Province (LR13C070001 and Y17C070004 to HY), the Fundamental Research Funds for the Central Universities, and to SY from NSFC (31370721). FW is a recipient of the National Thousand Young Talents Award.

Author contributions

CL and QC designed and performed the majority of the experiments and analysis, with the contributions from QY, MZ, HY, LZ, ZZ, and FQ. BZ and SY made the structural model of Wapl interaction with Haspin and Pds5B. FW conceived and supervised the project, analyzed the data, and wrote the manuscript.

Conflict of interest

The authors declare that they have no conflict of interest.

References

- Haering CH, Farcas AM, Arumugam P, Metson J, Nasmyth K (2008) The cohesin ring concatenates sister DNA molecules. *Nature* 454: 297–301
- Peters JM, Nishiyama T (2012) Sister chromatid cohesion. *Cold Spring Harb Perspect Biol* 4: a011130
- Waizenegger IC, Hauf S, Meinke A, Peters JM (2000) Two distinct pathways remove mammalian cohesin from chromosome arms in prophase and from centromeres in anaphase. *Cell* 103: 399–410
- Haarhuis JH, Elbatsh AM, Rowland BD (2014) Cohesin and its regulation: on the logic of X-shaped chromosomes. *Dev Cell* 31: 7–18

5. Ouyang Z, Zheng G, Song J, Borek DM, Otwinowski Z, Brautigam CA, Tomchick DR, Rankin S, Yu H (2013) Structure of the human cohesin inhibitor Wapl. *Proc Natl Acad Sci USA* 110: 11355–11360
6. Shintomi K, Hirano T (2009) Releasing cohesin from chromosome arms in early mitosis: opposing actions of Wapl-Pds5 and Sgo1. *Genes Dev* 23: 2224–2236
7. Gandhi R, Gillespie PJ, Hirano T (2006) Human Wapl is a cohesin-binding protein that promotes sister-chromatid resolution in mitotic prophase. *Curr Biol* 16: 2406–2417
8. Kueng S, Hegemann B, Peters BH, Lipp JJ, Schleiffer A, Mechtler K, Peters JM (2006) Wapl controls the dynamic association of cohesin with chromatin. *Cell* 127: 955–967
9. Chatterjee A, Zakian S, Hu XW, Singleton MR (2013) Structural insights into the regulation of cohesion establishment by Wpl1. *EMBO J* 32: 677–687
10. Chan KL, Roig MB, Hu B, Beckouet F, Metson J, Nasmyth K (2012) Cohesin's DNA exit gate is distinct from its entrance gate and is regulated by acetylation. *Cell* 150: 961–974
11. Ouyang Z, Zheng G, Tomchick DR, Luo X, Yu H (2016) Structural basis and IP6 requirement for Pds5-dependent cohesin dynamics. *Mol Cell* 62: 248–259
12. Rowland BD, Roig MB, Nishino T, Kurze A, Uluocak P, Mishra A, Beckouet F, Underwood P, Metson J, Imre R et al (2009) Building sister chromatid cohesion: smc3 acetylation counteracts an antiestablishment activity. *Mol Cell* 33: 763–774
13. Murayama Y, Uhlmann F (2015) DNA entry into and exit out of the cohesin ring by an interlocking gate mechanism. *Cell* 163: 1628–1640
14. Beckouet F, Srinivasan M, Roig MB, Chan KL, Scheinost JC, Batty P, Hu B, Petela N, Gligoris T, Smith AC et al (2016) Releasing activity disengages cohesin's Smc3/Sccl1 interface in a process blocked by acetylation. *Mol Cell* 61: 563–574
15. Eichinger CS, Kurze A, Oliveira RA, Nasmyth K (2013) Disengaging the Smc3/kleisin interface releases cohesin from *Drosophila* chromosomes during interphase and mitosis. *EMBO J* 32: 656–665
16. Buheitel J, Stemmann O (2013) Prophase pathway-dependent removal of cohesin from human chromosomes requires opening of the Smc3-Sccl1 gate. *EMBO J* 32: 666–676
17. Gligoris TG, Scheinost JC, Burmann F, Petela N, Chan KL, Uluocak P, Beckouet F, Gruber S, Nasmyth K, Lowe J (2014) Closing the cohesin ring: structure and function of its Smc3-kleisin interface. *Science* 346: 963–967
18. Nishiyama T, Ladurner R, Schmitz J, Kreidl E, Schleiffer A, Bhaskara V, Bando M, Shirahige K, Hyman AA, Mechtler K et al (2010) Sororin mediates sister chromatid cohesion by antagonizing Wapl. *Cell* 143: 737–749
19. Uhlmann F, Lottspeich F, Nasmyth K (1999) Sister-chromatid separation at anaphase onset is promoted by cleavage of the cohesin subunit Sccl1. *Nature* 400: 37–42
20. Uhlmann F, Wernic D, Poupart MA, Koonin EV, Nasmyth K (2000) Cleavage of cohesin by the CD clan protease separin triggers anaphase in yeast. *Cell* 103: 375–386
21. Hauf S, Waizenegger IC, Peters JM (2001) Cohesin cleavage by separase required for anaphase and cytokinesis in human cells. *Science* 293: 1320–1323
22. Barber TD, McManus K, Yuen KW, Reis M, Parmigiani G, Shen D, Barrett I, Nouhi Y, Spencer F, Markowitz S et al (2008) Chromatid cohesion defects may underlie chromosome instability in human colorectal cancers. *Proc Natl Acad Sci USA* 105: 3443–3448
23. Losada A (2014) Cohesin in cancer: chromosome segregation and beyond. *Nat Rev Cancer* 14: 389–393
24. McGuinness BE, Hirota T, Kudo NR, Peters JM, Nasmyth K (2005) Shugoshin prevents dissociation of cohesin from centromeres during mitosis in vertebrate cells. *PLoS Biol* 3: e86
25. Salic A, Waters JC, Mitchison TJ (2004) Vertebrate shugoshin links sister centromere cohesion and kinetochore microtubule stability in mitosis. *Cell* 118: 567–578
26. Kitajima TS, Sakuno T, Ishiguro K, Iemura S, Natsume T, Kawashima SA, Watanabe Y (2006) Shugoshin collaborates with protein phosphatase 2A to protect cohesin. *Nature* 441: 46–52
27. Tang Z, Shu H, Qi W, Mahmood NA, Mumby MC, Yu H (2006) PP2A is required for centromeric localization of Sgo1 and proper chromosome segregation. *Dev Cell* 10: 575–585
28. Nishiyama T, Sykora MM, Huis in 't Veld PJ, Mechtler K, Peters JM (2013) Aurora B and Cdk1 mediate Wapl activation and release of acetylated cohesin from chromosomes by phosphorylating Sororin. *Proc Natl Acad Sci USA* 110: 13404–13409
29. Liu H, Qu Q, Warrington R, Rice A, Cheng N, Yu H (2015) Mitotic transcription installs Sgo1 at centromeres to coordinate chromosome segregation. *Mol Cell* 59: 426–436
30. Hara K, Zheng G, Qu Q, Liu H, Ouyang Z, Chen Z, Tomchick DR, Yu H (2014) Structure of cohesin subcomplex pinpoints direct shugoshin-Wapl antagonism in centromeric cohesion. *Nat Struct Mol Biol* 21: 864–870
31. Liu H, Rankin S, Yu H (2013) Phosphorylation-enabled binding of SGO1-PP2A to cohesin protects sororin and centromeric cohesion during mitosis. *Nat Cell Biol* 15: 40–49
32. Liu H, Jia L, Yu H (2013) Phospho-H2A and cohesin specify distinct tension-regulated Sgo1 pools at kinetochores and inner centromeres. *Curr Biol* 23: 1927–1933
33. Kawashima SA, Yamagishi Y, Honda T, Ishiguro K, Watanabe Y (2010) Phosphorylation of H2A by Bub1 prevents chromosomal instability through localizing shugoshin. *Science* 327: 172–177
34. Lee J, Kitajima TS, Tanno Y, Yoshida K, Morita T, Miyano T, Miyake M, Watanabe Y (2008) Unified mode of centromeric protection by shugoshin in mammalian oocytes and somatic cells. *Nat Cell Biol* 10: 42–52
35. Tang Z, Sun Y, Harley SE, Zou H, Yu H (2004) Human Bub1 protects centromeric sister-chromatid cohesion through Shugoshin during mitosis. *Proc Natl Acad Sci USA* 101: 18012–18017
36. Dai J, Sullivan BA, Higgins JM (2006) Regulation of mitotic chromosome cohesion by Haspin and Aurora B. *Dev Cell* 11: 741–750
37. Zhou L, Liang C, Chen Q, Zhang Z, Zhang B, Yan H, Qi F, Zhang M, Yi Q, Guan Y et al (2017) The N-terminal non-kinase-domain-mediated binding of Haspin to Pds5B protects centromeric cohesion in mitosis. *Curr Biol* 27: 992–1004
38. Goto Y, Yamagishi Y, Shintomi-Kawamura M, Abe M, Tanno Y, Watanabe Y (2017) Pds5 regulates sister-chromatid cohesion and chromosome bi-orientation through a conserved protein interaction module. *Curr Biol* 27: 1005–1012
39. Dai J, Sultan S, Taylor SS, Higgins JM (2005) The kinase Haspin is required for mitotic histone H3 Thr 3 phosphorylation and normal metaphase chromosome alignment. *Genes Dev* 19: 472–488
40. Yamagishi Y, Honda T, Tanno Y, Watanabe Y (2010) Two histone marks establish the inner centromere and chromosome bi-orientation. *Science* 330: 239–243
41. Wang F, Dai J, Daum JR, Niedzialkowska E, Banerjee B, Stukenberg PT, Gorbisky GJ, Higgins JM (2010) Histone H3 Thr-3 phosphorylation by Haspin positions Aurora B at centromeres in mitosis. *Science* 330: 231–235

42. Kelly AE, Ghenoiu C, Xue JZ, Zierhut C, Kimura H, Funabiki H (2010) Survivin reads phosphorylated histone H3 threonine 3 to activate the mitotic kinase Aurora B. *Science* 330: 235–239
43. Wang F, Ulyanova NP, Daum JR, Patnaik D, Kateneva AV, Gorbsky GJ, Higgins JM (2012) Haspin inhibitors reveal centromeric functions of Aurora B in chromosome segregation. *J Cell Biol* 199: 251–268
44. De Antoni A, Maffini S, Knapp S, Musacchio A, Santaguida S (2012) A small-molecule inhibitor of Haspin alters the kinetochore functions of Aurora B. *J Cell Biol* 199: 269–284
45. Carmena M, Wheelock M, Funabiki H, Earnshaw WC (2012) The chromosomal passenger complex (CPC): from easy rider to the godfather of mitosis. *Nat Rev Mol Cell Biol* 13: 789–803
46. Carretero M, Ruiz-Torres M, Rodriguez-Corsino M, Barthelemy I, Losada A (2013) Pds5B is required for cohesion establishment and Aurora B accumulation at centromeres. *EMBO J* 32: 2938–2949
47. Riedel CG, Katis VL, Katou Y, Mori S, Itoh T, Helmhart W, Galova M, Petronczki M, Gregan J, Cetin B et al (2006) Protein phosphatase 2A protects centromeric sister chromatid cohesion during meiosis I. *Nature* 441: 53–61
48. Daum JR, Potapova TA, Sivakumar S, Daniel JJ, Flynn JN, Rankin S, Gorbsky GJ (2011) Cohesion fatigue induces chromatid separation in cells delayed at metaphase. *Curr Biol* 21: 1018–1024
49. Gorbsky GJ (2013) Cohesion fatigue. *Curr Biol* 23: R986–R988
50. Eswaran J, Patnaik D, Filippakopoulos P, Wang F, Stein RL, Murray JW, Higgins JM, Knapp S (2009) Structure and functional characterization of the atypical human kinase Haspin. *Proc Natl Acad Sci USA* 106: 20198–20203
51. Villa F, Capasso P, Tortorici M, Forneris F, de Marco A, Mattevi A, Musacchio A (2009) Crystal structure of the catalytic domain of Haspin, an atypical kinase implicated in chromatin organization. *Proc Natl Acad Sci USA* 106: 20204–20209
52. Maiolica A, de Medina-Redondo M, Schoof EM, Chaikuad A, Villa F, Gatti M, Jeganathan S, Lou HJ, Novy K, Hauri S et al (2014) Modulation of the chromatin phosphoproteome by the Haspin protein kinase. *Mol Cell Proteomics* 13: 1724–1740
53. Kettenbach AN, Wang T, Faherty BK, Madden DR, Knapp S, Bailey-Kellogg C, Gerber SA (2012) Rapid determination of multiple linear kinase substrate motifs by mass spectrometry. *Chem Biol* 19: 608–618
54. Fuchs SM, Krajewski K, Baker RW, Miller VL, Strahl BD (2011) Influence of combinatorial histone modifications on antibody and effector protein recognition. *Curr Biol* 21: 53–58
55. Lundby A, Lage K, Weinert BT, Bekker-Jensen DB, Secher A, Skovgaard T, Kelstrup CD, Dmytryiev A, Choudhary C, Lundby C et al (2012) Proteomic analysis of lysine acetylation sites in rat tissues reveals organ specificity and subcellular patterns. *Cell Rep* 2: 419–431
56. Dreier MR, Bekier ME, Taylor WR (2011) Regulation of sororin by Cdk1-mediated phosphorylation. *J Cell Sci* 124: 2976–2987
57. Zhang N, Panigrahi AK, Mao Q, Pati D (2011) Interaction of Sororin protein with polo-like kinase 1 mediates resolution of chromosomal arm cohesion. *J Biol Chem* 286: 41826–41837
58. Hauf S, Roitinger E, Koch B, Dittrich CM, Mechtler K, Peters JM (2005) Dissociation of cohesin from chromosome arms and loss of arm cohesion during early mitosis depends on phosphorylation of SA2. *PLoS Biol* 3: e69
59. Gimenez-Abian JF, Sumara I, Hirota T, Hauf S, Gerlich D, de la Torre C, Ellenberg J, Peters JM (2004) Regulation of sister chromatid cohesion between chromosome arms. *Curr Biol* 14: 1187–1193
60. Losada A, Hirano M, Hirano T (2002) Cohesin release is required for sister chromatid resolution, but not for condensin-mediated compaction, at the onset of mitosis. *Genes Dev* 16: 3004–3016
61. Sumara I, Vorlaufer E, Stukenberg PT, Kelm O, Redemann N, Nigg EA, Peters JM (2002) The dissociation of cohesin from chromosomes in prophase is regulated by Polo-like kinase. *Mol Cell* 9: 515–525
62. Niedzialkowska E, Wang F, Porebski PJ, Minor W, Higgins JM, Stukenberg PT (2012) Molecular basis for phosphospecific recognition of histone H3 tails by Survivin paralogues at inner centromeres. *Mol Biol Cell* 23: 1457–1466
63. Jeyapragash AA, Basquin C, Jayachandran U, Conti E (2011) Structural basis for the recognition of phosphorylated histone h3 by the survivin subunit of the chromosomal passenger complex. *Structure* 19: 1625–1634
64. Du J, Kelly AE, Funabiki H, Patel DJ (2012) Structural basis for recognition of H3T3ph and Smac/DIABLO N-terminal peptides by human Survivin. *Structure* 20: 185–195
65. Hengeveld RCC, Vromans MJM, Vleugel M, Hadders MA, Lens SMA (2017) Inner centromere localization of the CPC maintains centromere cohesion and allows mitotic checkpoint silencing. *Nat Commun* 8: 15542
66. Tsukahara T, Tanno Y, Watanabe Y (2010) Phosphorylation of the CPC by Cdk1 promotes chromosome bi-orientation. *Nature* 467: 719–723
67. Rankin S, Ayad NG, Kirschner MW (2005) Sororin, a substrate of the anaphase-promoting complex, is required for sister chromatid cohesion in vertebrates. *Mol Cell* 18: 185–200
68. Schmitz J, Watrin E, Lenart P, Mechtler K, Peters JM (2007) Sororin is required for stable binding of cohesin to chromatin and for sister chromatid cohesion in interphase. *Curr Biol* 17: 630–636
69. Lafont AL, Song J, Rankin S (2010) Sororin cooperates with the acetyltransferase Eco2 to ensure DNA replication-dependent sister chromatid cohesion. *Proc Natl Acad Sci USA* 107: 20364–20369
70. Trivedi P, Stukenberg PT (2016) A centromere-signaling network underlies the coordination among mitotic events. *Trends Biochem Sci* 41: 160–174